Desalination and Water Treatment
www.deswater.com
doi: 10.5004/dwt.2023.29172

282 (2023) 265–275
January

Preparation of NiFeCu-layered double hydroxide/graphene composite microsphere and its adsorption for dye from aqueous solution

Zhuannian Liu, Rui Zhou*, Yue Li, Wei Liu, Sheng Liao

College of Geology and Environment, Xi'an University of Science and Technology, Xi'an 710054, China, Tel. +86 15877594159; email: 1693376060@qq.com (R. Zhou), Tel. +86 13892803449; email: 2573484342@qq.com (Z. Liu), Tel. +86 15094005925; email: 1165748150@qq.com (Y. Li), Tel. +86 15602488170; email: 17322422444@qq.com (W. Liu), Tel. +86 15929561827; email: 56753515@qq.com (S. Liao)

Received 14 August 2022; Accepted 28 November 2022

ABSTRACT

Microspheric NiFeCu layered double hydroxide/graphene oxide (NiFeCu-LDH/GO) composites were prepared by one-pot hydrothermal method. Scanning electron microscopy showed that NiFeCu-LDH/GO was a porous microspheric structure. Nitrogen adsorption–desorption analysis showed that the addition of GO increased the specific surface area of NiFeCu-LDH from 34.61 to 113.64 m^2/g. The adsorption properties of Congo red by NiFeCu-LDH, NiFeCu-LDH/GO, GO and commercial activated carbon were studied. The results showed that the adsorption capacity of NiFeCu-LDH/GO is obviously better than that of the other three materials, when the temperature is 298.15 K and pH is 4, according to the Langmuir adsorption isothermal model, the theoretical maximum adsorption capacity is 867.67 mg/g, which was much larger than the maximum adsorption capacity of GONiFe-LDH composite for Congo red (421.35 mg/g). The kinetic and thermodynamic studies showed that the adsorption process of NiFeCu-LDH/GO composite for Congo red corresponded to the pseudo-second-order kinetic model and the Langmuir isothermal model, and the adsorption performance remained good after being reused for four times. These results indicated that the NiFeCu-LDH/GO composite had a strong potential for mitigating Congo red dye in wastewater.

Keywords: Adsorption; Congo red; Graphene oxide; Layered double hydroxide

1. Introduction

Dyes are mainly used in textile, dyeing, pharmaceutical, paper and, leather and paint industries. The impact is highly alarming as huge amount of dye containing wastewater is discharging into the environment each year without proper pretreatment [1]. Dyes reduce the light penetration in natural water bodies, affecting photo-synthetic activities and reduce dissolved oxygen, which threaten the life of aquatic species [2]. Dyes are classified in terms of structure, application methods and ionic nature [3]. When classified on the basis of structure, these are studied as azo, anthraquinone, indigoid, nitroso, nitro and triarylmethane [4]. Congo red is an example of a diazo dye, which is prepared by coupling tetrazolium benzidine with two molecules of naphthoic acid. It can cause a variety of health problems for people and animals, including breathing difficulties, vomiting, diarrhea and nausea [5]. In addition, Congo red have high toxicity, stable chemical properties, and complex structures, which are highly carcinogenic, teratogenic, and mutagenic to humans and other organisms [6–8].

Various methods have been utilized to treat dye wastewater, for example, adsorption, particle trade, coagulation/

* Corresponding author.

flocculation, film filtration, electrochemical techniques, photocatalysis, and biodegradation [9–12]. Among them, adsorption method is considered to be the most promising and advantageous method for removing dyes, due to it high efficiency, simple operation and separation, easy regeneration, and good selectivity [12,13]. Various adsorbents, such as activated carbon [14], biochar, resin, zeolite [15], metal organic framework materials, have been widely used to treat dye wastewater. Nonetheless, the use of these adsorbents is restricted by certain elements, such as, high cost, low adsorption capacity, and troublesome recovery. Therefore, developing new adsorbents with low cost, higher adsorption performance, and good reusability is high required.

Graphene oxide (GO) is the result of the substance oxidation and peeling of graphite powder [16]. It has a high specific surface and consist with many oxygen-containing functional groups on its surface and edge, like hydroxyl (–OH), carboxyl (–COOH), carbonyl (–C=O–). Presence of these functional groups on the surface of the GO is beneficial for the adsorption of specific toxic elements in wastewater [17,18]. On the other land, layered double hydroxides (LDHs), also called hydrotalcite, are a sort of layered structure material made out of a decidedly charged fundamental layer and adversely charged interlayer anions. The general formula can be expressed as $[M^{2+}_{1-x}M^{3+}_{x}(OH)_2]^{x+}(A^{n-})_{x/n}\ mH_2O$, where M^{2+} is a divalent cation, for example, Cu^{2+}, Co^{2+} or Ni^{2+}; M^{3+} is a trivalent cation, such as Cr^{3+}, Al^{3+} or Fe^{3+}, A^{n-} is anion, like CO_3^{2-}, NO_3^- and Cl^- [19–24]. Because of its huge explicit surface area, amazing particle trade execution, requested layered design and high controllability of structure, it has drawn in extraordinary attention by the researchers. A progression of hydrotalcites with various morphologies and their calcined items have been effectively arranged and used to eliminate numerous natural and inorganic poisons in real wastewater. However, it is difficult to separate GO directly from water due to its good dispersion and hydrophilicity. To facilitate the separation of GO from the liquid phase, LDH is used as a coagulant to remove GO. Therefore, GO-LDH composites are considered to be an adsorbent that can be easily separated from water [24–28]. Therefore, this paper reported the adsorption performance of NiFeCu layered double hydroxide/graphene oxide (NiFeCu-LDH/GO) composites on Congo red in simulated wastewater.

In this study, a one-pot hydrothermal method was used to prepare microspherical NiFeCu-LDH/GO composites for adsorption of Congo red in simulated wastewater. The materials were characterized and analyzed using scanning electron microscopy (SEM), X-ray diffraction (XRD), Fourier-transform infrared spectroscopy (FT-IR), X-ray photoelectron spectroscopy (XPS), BET and EDS. The effects of NiFeCu-LDH/GO composites on the adsorption performance of Congo red (CR) under different influencing factors were discussed. In order to study the adsorption process and adsorption mechanism, the adsorption kinetics, adsorption isotherms and adsorption thermodynamics were studied. The results showed that the NiFeCu-LDH/GO composite was successfully synthesized, and it had a strong adsorption capacity for CR removal in simulated wastewater.

2. Materials and methods

2.1. Materials

The chemicals used to prepare NiFeCu-LDH/GO composites include ferric nitrate nonahydrate ($Fe(NO_3)_3{\cdot}9H_2O$), nickel nitrate hexahydrate ($Ni(NO_3)_2{\cdot}6H_2O$), copper nitrate hexahydrate ($Cu(NO_3)_2{\cdot}6H_2O$) urea ($CO(NH_2)_2$) and ammonium fluoride (NH_4F), all purchased from China Pharmaceutical Chemicals Co., Ltd., (China). Chemicals used to prepare graphene oxide include graphite powder (C, CP, ≥99.85%), sulfuric acid (H_2SO_4, AR, 95–98 wt.%), sodium nitrate ($NaNO_3$, AR, ≥99.0%),potassium permanganate ($KMnO_4$, AR, ≥95%), hydrogen peroxide (H_2O_2, AR, 30 wt.%) and hydrochloric acid (HCl, AR, 36–38 wt.%),which were bought from China Pharmaceutical Chemicals Co., Ltd. Activated carbon was purchased from Wuxi Yatai United Chemical Co., LTD. Ethanol and Congo red ($C_{32}H_{22}N_6Na_2$) were all analytically pure, and the experimental water is deionized.

2.2. Preparation and characterization of GO and NiFeCu-LDH/GO

Preparation of GO: In a 0°C~5°C ice bath,5 g graphite powder,15 g potassium permanganate, and 2.5 g nitric acid were slowly added into a 500 mL beaker containing 115 mL concentrated sodium sulfate and continuously stirred for 1 h. Then, the temperature was adjusted to 35°C and kept stirring for 3 h. Next, rising the temperature to 85°C and slowly add 230 mL ultra-pure water, mixed for 15 min. At room temperature, after adding 5 mL hydrogen peroxide, stirred for extra 1 h. Following that, the mixture was soaked in 5% hydrochloric acid overnight, washed with 0.1 mol/L hydrochloric acid for 4 times, and washed with deionized water for several times till the pH become neutral. Consequently, it was oven dried at 60°C for 12 h.

Preparation of NiFeCu-LDH/GO composite: 3.534 g $Fe(NO_3)_3{\cdot}9H_2O$, 6.359 g $Ni(NO_3)_2{\cdot}6H_2O$, 2.035 g $Cu(NO_3)_2$ $6H_2O$, 6.306 g $CO(NH_2)_2$, 0.5 g GO and 1.943 g NH_4F was added to 75 mL of deionized water and stirred for 40 min until completely dissolved. The mixture was poured into a 100 mL Teflon reactor and reacted in an oven at 90°C for 12 h. After cooling to 25°C, the mixture was taken out, centrifuged, washed 6 times with ethanol and deionized water, and then dried in an oven at 60°C for 12 h. Samples were stored for subsequent experiments.

The characterization of NiFeCu-LDH/GO composite was performed using Sigma500 electron microscope of ZEISS in Germany to observe the surface results and pore characteristics in composite microstates. XD-3 X-ray diffractometer was used to measure the crystal diffraction of composite materials. The measurement conditions were Kα-ray of copper target and wavelength λ = 0.15418 nm. The scanning voltage is 36 kV, the scanning current is 20 mA, and the scanning step is 0.02°, and the scanning range is 5°~80°. Infrared test using PerkinElmer 550S Fourier transform infrared spectrometer, scanning test wave number 4,000~500 cm^{-1}. In this experiment, JWBK122W nitrogen physical adsorption instrument (Beijing Jinweige Technology Co., Ltd.) was used to test the specific surface area, pore volume and pore size of the adsorption

composite material. ESCALAB 250Xi X-ray photoelectron spectroscopy and Auger electron spectrometer Themo Fisher Corporation of the United States were used to determine the valence state of surface elements before and after the adsorptionof CR.

2.3. Experimental section

In order to study the adsorption performance of NiFeCu-LDH/GO on Congo red, a CR solution with a concentration of 500 mg/L was prepared and placed in a volumetric flask. Then, take 50 mL solution into 100 mL conical flask, add 0.1 g adsorbent, place it into the shaker at 25°C under 150 rpm. The sample were taking out at different times. The UV-6100 S dual-beam spectrophotometer was used to analyze the UV-visible spectrum at 497 nm. The absorbance of the solution after adsorption was measured at 497 nm in a 10 mm cuvette and the concentration was calculated according to the standard curve. By adjusting the pH value of CR-containing wastewater, the temperature of the shaker and the initial concentration of CR wastewater, the effects of adsorbents on the adsorption process under different influencing factors were studied. The calculation formulas of removal rate and adsorption capacity are as follows:

$$q_e = \frac{(C_0 - C_e)V}{m} \tag{1}$$

where q_e is the adsorption capacity at adsorption equilibrium; C_0 is the initial concentration of CR wastewater, mg/L; C_e is the CR wastewater concentration at adsorption equilibrium, mg/L; V is the volume of CR wastewater, L; m is the mass of the adsorbent; g. And η is the removal rate, %; C_0 is the initial concentration of CR solution, mg/L; C_t is the mass concentration of CR after adsorption, mg/L.

3. Results and discussion

3.1. Morphology and microstructure

Fig. 1a and b are the SEM images of NiFeCu-LDH. It can be seen that NiFeCu-LDH was a thick lamellar structure with many wrinkles and uneven surfaces formed by disordered stacking. Further amplification can be seen that these lamellar structures agglomerate to form interconnected coral-like rugged surfaces. Fig. 1c and d are the SEM images of NiFeCu-LDH/GO composite. The addition of GO in NiFeCu-LDH/GO composite led to the stacking of these sheets and the formation of many wrinkled spheres. After further amplification, it can be seen that the morphology of these spheres, resulting to a larger specific surface area compared with NiFeCu-LDH and thus may have a larger adsorption capacity.

In addition, the element distribution of NiFeCu-LDH/GO composite was analyzed. Fig. 1e and f show the element distribution diagrams of Ni, Fe and Cu, respectively, showing a uniform distribution of the elements on the surface of the NiFeCu-LDH/GO composite, resulting to the successful synthesis of the NiFeCu-LDH/GO composite.

3.2. Crystal structure

Fig. 2 shows the XRD pattern of the samples. It can be seen from the figure that there are obvious diffraction peaks at 2θ = 12.9°, 18.8°, 23°, 33.5°, 36.4°, 38.5° and 47.2° [29,30]. And NiFeCu-LDH and NiFeCu-LDH/GO composite had the same diffraction peaks at the same position, which indicate the successful synthesis of the composite material. In addition, the addition of GO did not alter the diffraction peaks of NiFeCu-LDH/GO composite, which may be caused by the structure of GO, when GO is added to NiFeCu-LDH, and the masking of the characteristic peak of GO led to the unobvious characteristic peak.

3.3. Fourier transform infrared spectroscopy analysis

Fig. 3 shows the FT-IR spectra of NiFeCu-LDH/GO, NiFeCu-LDH and NiFeCu-LDH/GO before and after CR adsorption, respectively. For the three samples, 1,645 and 1,126 cm^{-1} are the vibrational peaks for C=O and C–N, respectively [31,32]. Among them, the strong peaks at 1,651 and 3,439 cm^{-1} correspond to H–O–H and O–H vibrations, respectively, the peaks at 2,845–2,950 cm^{-1} are caused by the vibration of C–H bonds, and the peak at 1,357 cm^{-1} is associated with –COOH vibration peak. When GO was added into NiFeCu-LDH/GO composite, the peak intensity become stronger compare to that of NiFeCu-LDH, and the vibrational peaks below 1,000 cm^{-1} are related to the vibrational peaks of Ni–O, Cu–O and Fe–O bonds.

3.4. Nitrogen adsorption–desorption analysis

The specific surface area, pore size and pore distribution of NiFeCu-LDH/GO, GO and NiFeCu-LDH were obtained by N_2 adsorption–desorption isotherm. From the N_2 adsorption–desorption curve in Fig. 4, it can be seen that GO, NiFeCu-LDH and NiFeCu-LDH/GO composites, has IV typical isotherms with mesoporous structure. The results are shown in Table 1. indicate that GO, NiFeCu-LDH and NiFeCu-LDH/GO composites have a pore size of 18.42, 5.55 and 3.08 nm, respectively. Through the changing trends of the adsorption–desorption isotherms of NiFeCu-LDH/GO and NiFeCu-LDH in Fig. 4, the adsorption hysteresis loop is H4 type, indicating that the composite adsorbent has microporous and mesoporous structure. The addition of GO weakened the effect of disordered stacking of NiFeCu-LDH, made the arrangement of NiFeCu-LDH/GO composites more orderly and formed microspheres structure, as well as increasing the specific surface area of the composite material to 113.64 m^2/g, while the specific surface area of GO and NiFeCu-LDH were 3.93, 34.61 m^2/g, respectively which was beneficiation for the adsorption of the pollutant.

3.5. XPS analysis

XPS was used to analyze the chemical state and elemental composition of NiFeCu-LDH/GO composites before and after CR adsorption. The recorded spectra are shown in Fig. 5a, which shows the peaks of Ni, Fe and Cu present in the measurement spectrum of NiFeCu-LDH/GO composites

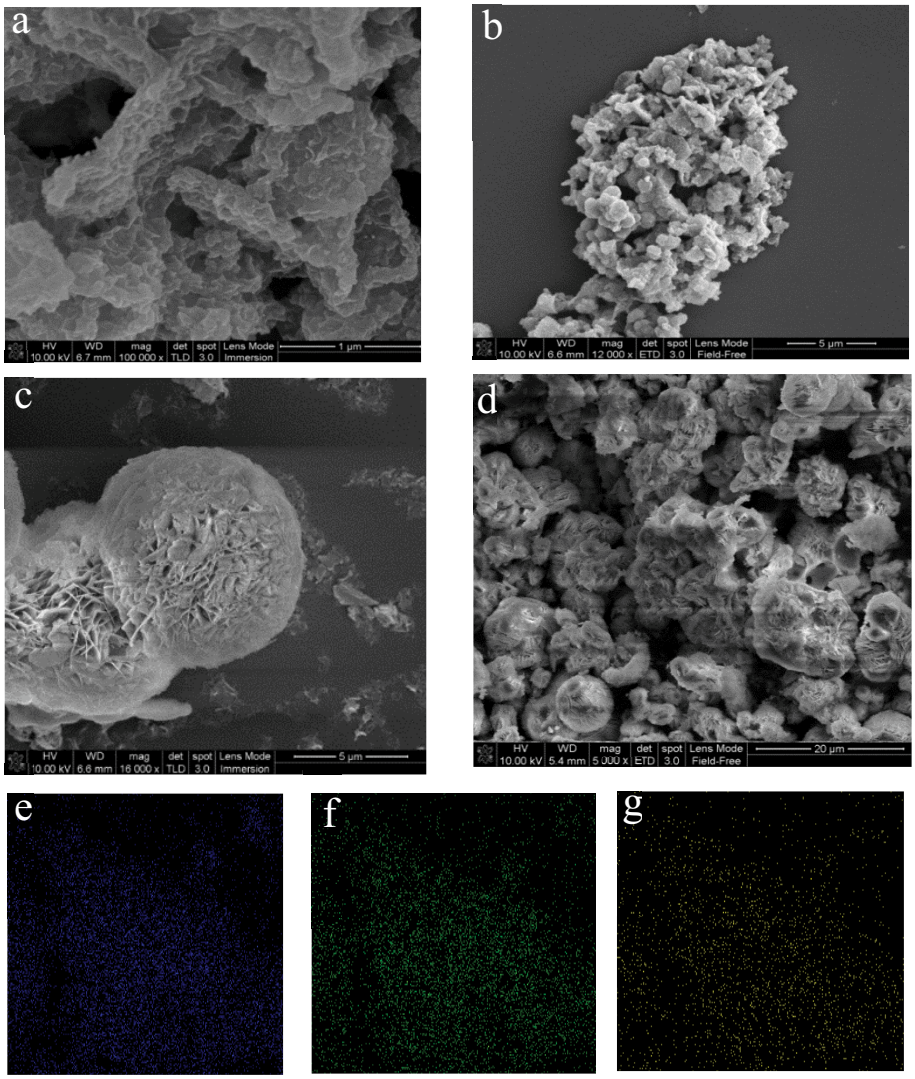

Fig. 1. (a, b) SEM image of NiFeCu-LDH, (c, d) SEM image of NiFeCu-LDH/GO, (e–g) illustrate the element distribution map of NiFeCu-LDH/GO composite, (e) Ni, (f) Fe, and (g) Cu.

before adsorption, indicating the successful preparation of NiFeCu-LDH/GO composites. In addition to the peaks of Ni, Fe, Cu, C, O, and N elements after adsorption, the peak of S also appeared in measurement, indicating that CR was successfully adsorbed on the surface of the material. Fig. 5b shows the comparison of Ni 2p high resolution regions before and after NiFeCu-LDH/GO composite adsorption, accordingly that there are four peaks, two peaks at 855.9 and 873.4 eV are from Ni $2p_{3/2}$ and Ni $2p_{1/2}$ core energy levels respectively, while the other two peaks are satellite peaks, which indicates that Ni in NiFeCu-LDH/GO is in bivalent form. In Fig. 5c, there are two peaks at 712.2 and 724.9 eV peaks, which are from Fe $2p_{3/2}$ and Fe $2p_{1/2}$ core energy levels. This result shows that Fe exists in NiFeCu-LDH/GO in the form of trivalent [10,33]. Similarly, for Cu 2p spectrum (Fig. 5d), the peaks of 954.8 eV and 934.9 eV are from Cu $2p_{1/2}$ and Cu $2p_{3/2}$, and the remaining two peaks are satellite peaks, which indicates that Cu in NiFeCu LDH/GO is in bivalent form [34].

3.6. Effect of time on adsorption effect

Fig. 6 shows the comparison of the adsorption capacities of the composite material in different time for CR. It can be seen from the figure that the adsorption capacity rate of our composite material was very fast in the first 30 min. It was presence of a large number of adsorption sites on the surface of the material, so that the material can quickly adsorb CR. With the increase of adsorption time, a large number of adsorption sites were gradually occupied by CR, the adsorption rate slowed down, and the adsorption equilibrium was finally reached at about 200 min. By comparing the adsorption capacities of NiFeCu-LDH/GO, NiFeCu-LDH, GO, and active carbon to CR, it can be seen that the adsorption capacity of NiFeCu-LDH/GO to CR much higher than other materials. In order to compare the adsorption rates of NiFeCu-LDH/GO, GO, active carbon and NiFeCu-LDH for CR, the Lagergren pseudo-first-order reaction kinetic model and pseudo-second-order reaction kinetic

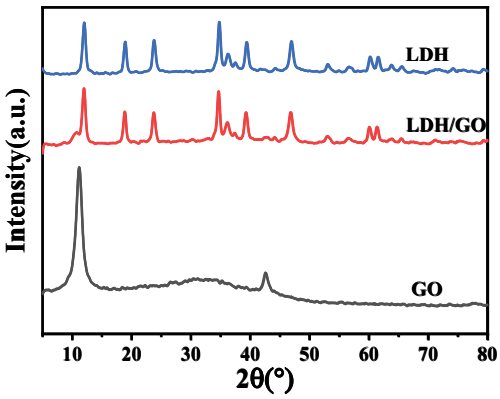

Fig. 2. X-ray diffraction patterns of samples.

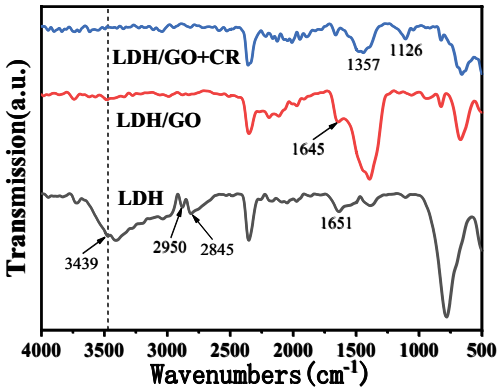

Fig. 3. FT-IR spectra of samples.

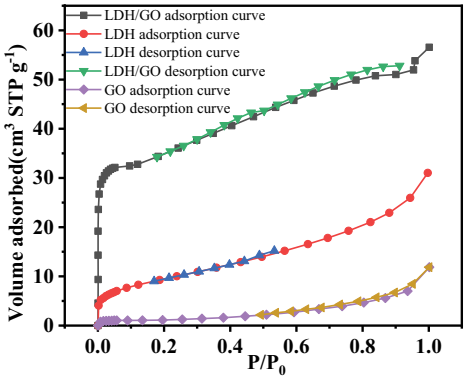

Fig. 4. N_2 adsorption–desorption isotherms.

model were used to compare the two adsorption materials. The form of the Lagergren pseudo-first-order adsorption kinetic equation is calculated as follows:

$$\log\left(q_e - q_t\right) = \log q_e - \frac{k_1}{2.303}t \tag{2}$$

where q_t is the adsorption capacity of time t, mg/g; q_e is equilibrium adsorption capacity, mg/g; k_1 is the pseudo-first-order adsorption rate constant, min^{-1}.

The pseudo-second-order adsorption kinetic equation was calculated as follows:

$$\frac{t}{q_t} = \frac{1}{k_2 q_e^2} + \frac{1}{q_e}t \tag{3}$$

where q_t is the adsorption capacity of time t, mg/g; q_e is equilibrium adsorption capacity, mg/g; k_2 is the pseudo-second-order adsorption rate constant, g/mg·min.

The fitting results of the Lagergren pseudo-first-order and pseudo-second-order reaction rate equations are shown in Fig. 7, and the relevant parameters are shown in Table 2.

3.7. Adsorption isotherm

The adsorption isotherm can reflect the relationship between the adsorption capacity of the adsorbent and the concentration of the pollutant in the aqueous phase at the adsorption equilibrium. Fig. 8 shows the adsorption isotherms of CR on NiFeCu-LDH/GO composites, GO, active carbon and NiFeCu-LDH. It can be seen from the figure that the NiFeCu-LDH/GO composite exhibits higher adsorption capacity for CR than NiFeCu-LDH, GO, active carbon. The data were fitted using the Langmuir isotherm model and the Freundlich isotherm model as shown in Fig. 8. The fitting results are shown in Fig. 8. The relevant regression parameters were shown in Table 3. From Table 3, it can be seen that the linear correlation coefficient R^2 of the Langmuir adsorption isotherm of CR on NiFeCu-LDH/GO was larger than the linear correlation coefficient R^2 of the Freundlich isotherm of CR on NiFeCu-LDH/GO, which indicates that CR on NiFeCu-LDH/GO had a higher linear correlation coefficient R^2. The NiFeCu-LDH/GO composite best fit with the Langmuir isotherm model, which indicated that the adsorption was consistent with monolayer adsorption. According to the Langmuir isotherm equation, it can be concluded that the theoretical maximum adsorption capacity of CR by NiFeCu-LDH/GO composites is 867.669 mg/g. In addition, the adsorption capacities of different adsorbent materials with NiFeCu-LDH/GO composite for CR removal were compared. It can be seen from Table 4 that the adsorption capacity of NiFeCu-LDH/GO composites for CR removal was much larger than that of other adsorption adsorbents.

The Langmuir isotherm equation is

$$q_e = \frac{Q_0 K_L C_e}{1 + K_L C_e} \tag{4}$$

where Q_0 is the unit saturated adsorption amount when monolayer adsorption is formed, mg/g; C_e is the equilibrium mass concentration of the solution, mg/L; q_e is the equilibrium adsorption amount, mg/g; K_L is the Langmuir equilibrium constant.

The Freundlich isotherm equation is:

$$q_e = K_F C_e^{1/n} \tag{5}$$

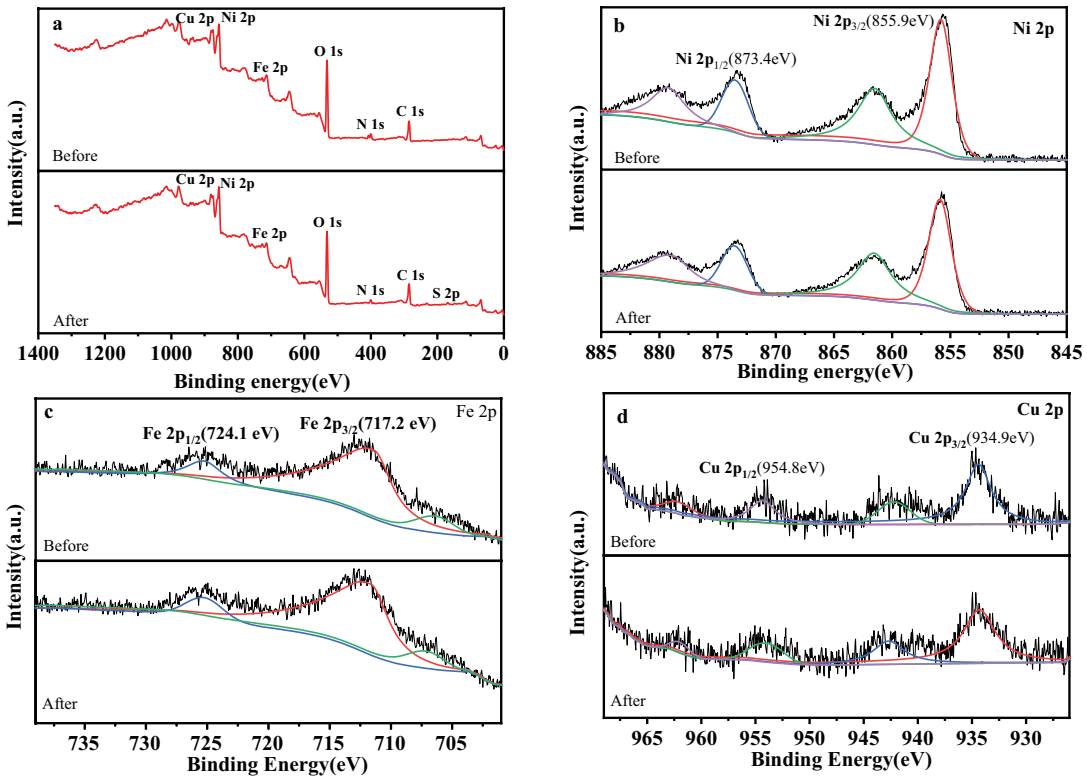

Fig. 5. XPS spectrum of NiFeCu-LDH/GO composite before and after CR adsorption (a) full spectrum; high resolution X-ray photoelectron spectroscopy of (b) Ni 2p regions, (c) Fe 2p regions, and (d) Cu 2p regions.

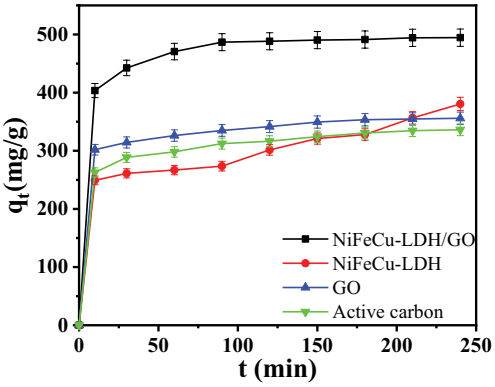

Fig. 6. Effect of adsorption time on adsorption effect.

where K_F and n are adsorption constants related to temperature and specific surface area of adsorbent.

3.8. Adsorption thermodynamics

Fig. 9 shows the effect of temperature on the adsorption capacity of CR by NiFeCu-LDH/GO, GO, active carbon and NiFeCu-LDH. It can be seen from the figure that with the gradual increase of temperature, the adsorption capacity of the adsorbent for CR removal gradually decreased. Therefore, higher temperature was not conducive to the adsorption of CR by the adsorbent, which might be due to the reaction of the adsorbent in higher temperature, resulting in poor adsorption. In order to explore a deeper understanding of the effect of temperature on the adsorption capacity, a thermodynamic model was used to fit the CR adsorption process of NiFeCu-LDH/GO, GO, active carbon and NiFeCu-LDH, and the fitted data are shown in Fig. 10. The relevant thermodynamic parameters were calculated according to the following equations.

Table 1
Pore characteristics of GO, NiFeCu-LDH/GO and NiFeCu-LDH

Sample	S_{BET} (m^2/g)	V_p (cm^3/g)	d_p (nm)
NiFeCu-LDH/GO	113.64	0.09	3.08
NiFeCu-LDH	34.61	0.05	5.55
GO	3.93	0.02	18.42

$$\Delta G = \Delta H - T\Delta S \tag{6}$$

where ΔG is Gibbs free energy change, J/mol; ΔH is the change of adsorption enthalpy, J/mol; ΔS is the change of adsorption entropy, J/K·mol; T is thermodynamic temperature, K; ΔH and ΔS are calculated as follows:

$$\log K_d = \frac{\Delta S}{R} - \frac{\Delta H}{2.303RT} \tag{7}$$

where K_d is the distribution coefficient and R is the thermodynamic constant, taking 8.314 J/K·mol.

The fitting results of the adsorption thermodynamic model is shown in Fig. 10, and the relevant parameters are shown in Table 5. It can be seen from Table 5 that both ΔH and ΔS during the adsorption of CR on NiFeCu-LDH/GO are negative, indicating that the sample NiFeCu-LDH/GO composite adsorption of CR is an exothermic reaction, which is consistent with Fig. 10 showed that the adsorption capacity of NiFeCu-LDH/GO composites for CR removal decreased with increasing temperature, and the ΔG was negative, indicating that the adsorption process was spontaneous.

3.9. Effect of pH and zeta potential test

The pH of the solution containing pollutants had obvious influence on the adsorption process. Therefore, the experiment of pH on the adsorption capacity of the solution was controlled at pH 2–10, as shown in Fig. 11 was drawn. It can be seen from Fig. 11 that with the increase of pH, the adsorption capacity of NiFeCu-LDH/GO, GO, active carbon and NiFeCu-LDH on CR removal gradually decreased, and the adsorption capacity was higher at pH = 4. When the pH value of the solution containing CR was low, the surface of NiFeCu-LDH/GO was positively charged and easily adsorbed CR, however, as the pH value increased, CR was not easily adsorbed. This might be due the positive charges on the surface of the NiFeCu-LDH/GO composite that were occupied by OH^- ions in the solution, resulting

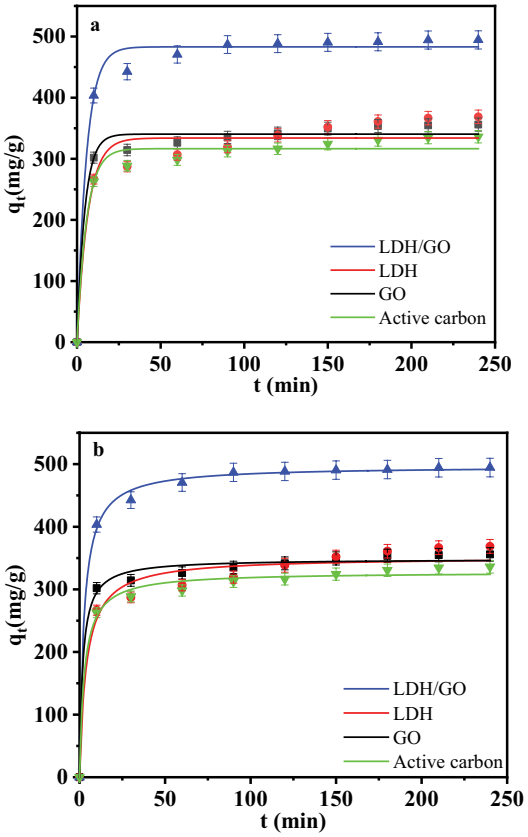

Fig. 7. Lagergren (a) first-order and (b) second-order kinetics equation plot.

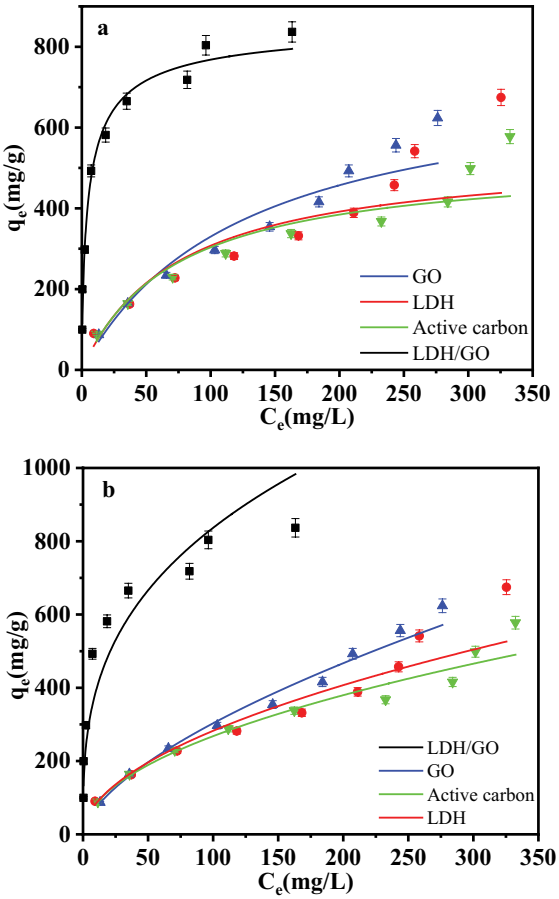

Fig. 8. Adsorption isotherms of CR adsorption on GO, active carbon, NiFeCu-LDH/GO and NiFeCu-LDH, (a) Langmuir and (b) Freundlich.

Table 2
Parameters in two kinetic models of GO, activated carbon, NiFeCu-LDH/GO composites and NiFeCu-LDH adsorbing CR

Adsorption material	Pseudo-first-order model			Pseudo-second-order model		
	k_1 (min^{-1})	q_e (mg/g)	R^2	k_2 (g/mg·min)	q_e (mg/g)	R^2
NiFeCu-LDH/GO	0.1762	483.055	0.9903	0.00079	496.783	0.9982
NiFeCu-LDH	0.2156	340.320	0.9982	0.00072	361.011	0.9837
GO	0.1528	333.879	0.9928	0.00157	348.638	0.9992
Activated carbon	0.1735	316.524	0.9974	0.0011	327.666	0.9989

Table 3
Comparison of CR adsorption capacity between NiFeCu-LDH/GO composite and other adsorbents

Adsorption material	Temperature	pH	Adsorption quantity (mg/g)	References
NiFeCu-LDH/GO	25°C	4	979	This work
NiFe-LDO	30°C	6	330	[10]
NiO/Graphene nanosheets	25°C	7	124	[35]
GO-NiFe LDH	30°C	6	489	[36]
α-FeOOH nanorods	30°C	7	160	[37]

Table 4
Langmuir and Freundlich isotherm model fitting parameters of adsorption isotherms of CR on GO, active carbon, NiFeCu-LDH/GO and NiFeCu-LDH

Adsorption material	Langmuir			Freundlich		
	Q_0	b	R^2	K_F	n	R^2
NiFeCu-LDH/GO	867.669	0.3027	0.9653	183.720	0.3292	0.9028
NiFeCu-LDH	539.919	0.0132	0.8735	24.963	0.5269	0.9626
GO	544.273	0.0079	0.9594	17.159	0.6236	0.9923
Active carbon	524.418	0.0137	0.9414	26.433	0.5029	0.9827

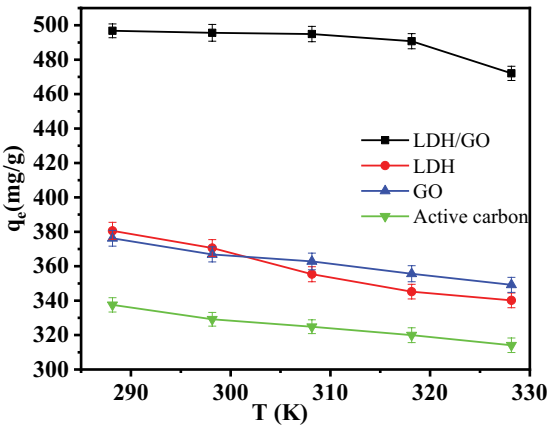

Fig. 9. Effects of different temperatures on CR adsorption.

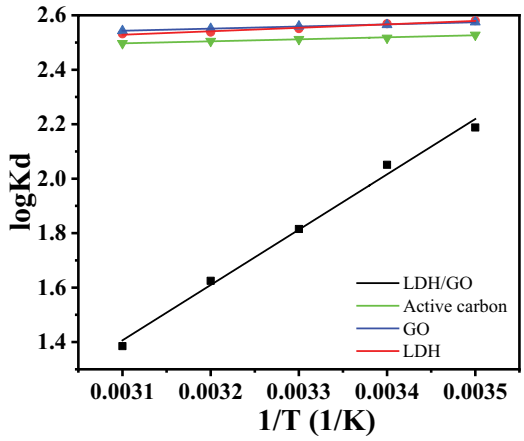

Fig. 10. The logK_d~1/T relation diagram of CR adsorbed by adsorbent.

Table 5
Thermodynamic parameters of adsorption of CR on GO, active carbon, NiFeCu-LDH and NiFeCu-LDH/GO composites

Adsorbents	T (K)	ΔG (kJ/mol)	ΔH (kJ/mol)	ΔS (J/K·mol)
NiFeCu-LDH/GO	288.15	–27.19	–38.91	–40.68
	298.15	–26.78		
	308.15	–26.38		
	318.15	–25.97		
	328.15	–25.56		
NiFeCu-LDH	288.15	–19.21	–24.32	17.75
	298.15	–19.03		
	308.15	–18.85		
	318.15	–18.67		
	328.15	–18.50		
GO	288.15	–7.01	–1.49	19.13
	298.15	–7.19		
	308.15	–7.38		
	318.15	–7.58		
	328.15	–7.77		
Active carbon	288.15	–6.85	–1.42	18.85
	298.15	–7.04		
	308.15	–7.23		
	318.15	–7.42		
	328.15	–7.61		

in a weakened attraction to CR, and reduce the adsorption capacity of the adsorbent.

It can be seen from Fig. 12 that the zeta potential of NiFeCu-LDH and NiFeCu-LDH/GO are 7.64 and 8.63, respectively, indicating that the surface of NiFeCu-LDH/

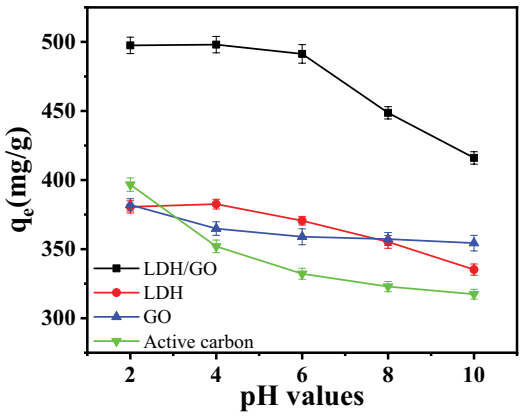

Fig. 11. Effect of pH on adsorption of CR onto samples.

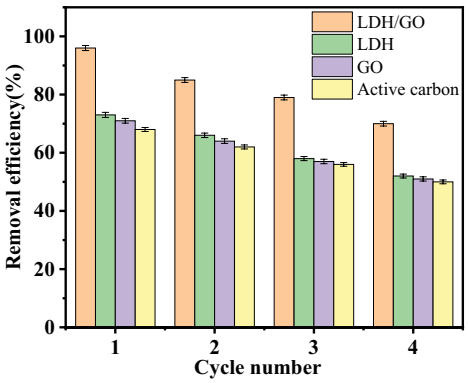

Fig. 13. Regeneration cycles of samples.

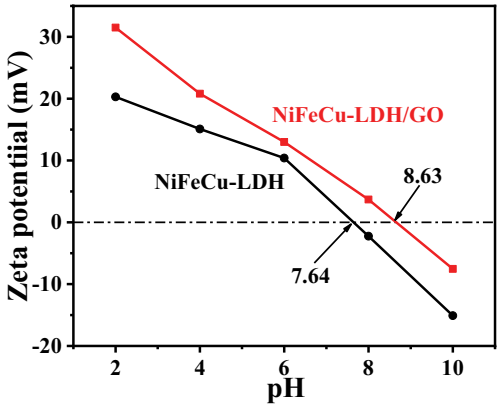

Fig. 12. Zeta potential of NiFeCu-LDH/GO and NiFeCu-LDH.

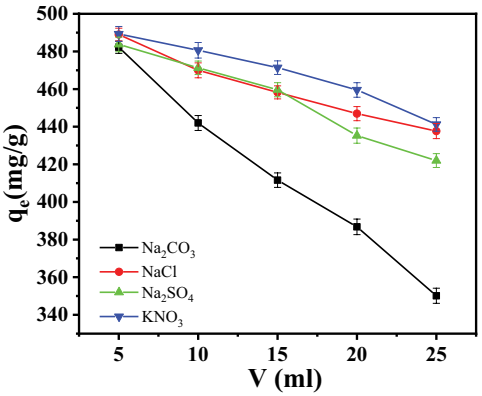

Fig. 14. Effect of different volume salt solution on adsorption capacity.

GO is positively charged when the pH is less than 8.63, and the surface is negatively charged when the pH is greater than 8.63. Moreover, the zeta potential larger between pH 2–4, indicating that NiFeCu-LDH/GO had better dispersibility and no agglomeration, so the adsorption capacity was higher at pH 2–4, which was related to the effect of pH on the adsorption capacity. In summary the pH at 2–4 was favorable for the adsorption of CR by the sorbent.

3.10. Regeneration and reuse

Reusability of the adsorbent is important for the practical use of materials. Therefore, this study investigated the reusability of NiFeCu-LDH/GO on CR. In order to regenerate the NiFeCu-LDH/GO composite, 0.1 mol/L NaOH was used for the desorption of the sample adsorbed CR by NiFeCu-LDH/GO. As shown in Fig. 13, after four adsorption–desorption cycles, the removal rate of CR by NiFeCu-LDH/GO remained at 70%, indicating that NiFeCu-LDH/GO material had good reusability.

3.11. Effect of saline CR wastewater on adsorption

For this purpose, different concentration of NaCl, Na_2SO_4, Na_2CO_3 and KNO_3 were added in 100 mg/L of CR simulated wastewater to explore the adsorption capacity of NiFeCu-LDH/GO on CR removal in presence of competing ions. As shown in Fig. 14, with the increase in the concentration of salts, the adsorption capacity of NiFeCu-LDH/GO on CR removal significantly decreased, among them Na_2CO_3 had a great influence on reduction of the adsorbent removal capacity. It might be due to the alkalinity of CO_3^{2-} and its hydrolysis in water, which reduces the adsorption capacity. Although the adsorption capacity of NiFeCu-LDH/GO for CR decreases after adding salt solution competing ions, it can still reach 350 mg/g, indicating that NiFeCu-LDH/GO can be used as a potential adsorbent for CR removal from aqueous solution.

3.12. Adsorption mechanism

As shown in Fig. 11, with the increase of solution pH, the adsorption amount of CR on NiFeCu-LDH/GO decreased, indicating that the positive charges on the surface of NiFeCu-LDH/GO had electrostatic attraction with the anionic dye CR. In addition, NiFeCu-LDH in NiFeCu-LDH/GO had an inherent ion exchange effect between layers, so the anionic dye CR could be adsorbed by ion-exchange with NiFeCu-LDH in the composite. However, GO in NiFeCu-LDH/GO contained a benzene ring, so Π–Π stacking occurred between GO and the benzene ring contained in CR, which enhanced the adsorption capacity of

the composite for CR removal. In addition, GO was rich in –OH, –COOH, These functional groups would form hydrogen bonds with $–NH_2$ contained in CR ions, thereby increasing the adsorption capacity of the composite material. Therefore, the adsorption mechanisms for CR removal by NiFeCu-LDH/GO included electrostatic interaction, ion exchange, Π–Π stacking, and hydrogen bonding.

4. Conclusion

In this study, a microsphere NiFeCu-LDH/GO composites were prepared by a one-pot hydrothermal method. The addition of GO in the material made the arrangement of NiFeCu-LDH/GO composites more disordered, forming a microsphere, which increased the specific surface area and increases the porosity. The results showed that the increased porosity and larger specific surface area and porosity, resulting to higher adsorption capacity of the composite material compare to that of NiFeCu-LDH material. The results of adsorption kinetics, adsorption isotherm and showed that the adsorption of NiFeCu-LDH/GO composites reach to equilibrium at 4h with the maximum adsorption capacity of 867.66 mg/g based on the Langmuir isotherm and the adsorption was spontaneous and endothermic. The adsorption capacity of NiFeCu-LDH/GO composite was much higher than that of NiFe-LDH (421.35 mg/g), GO and commercial activated carbon for Congo red removal. It was found that competing co-existing ions slightly reduce the adsorption capacity of the composite material. After four adsorption–desorption cycles, the composite still had 70% adsorption capacity, indicating that this composite be reused as a good adsorbent for CR adsorption. Although the material synthesized in this study has a high adsorption capacity and still maintains a high adsorption ability in saline wastewater, the synthesis temperature of this material is higher than room temperature, and metal elements are added, resulting in higher costs.

Acknowledgement

The research was supported by the Science and Technology Planning Project of Shaanxi Provincial Water Resources Department (2022slkj-5), and Shaanxi provincial Science and Technology Planning Project (2022SF-578).

References

[1] J. Mittal, Recent progress in the synthesis of layered double hydroxides and their application for the adsorptive removal of dyes: a review, J. Environ. Manage., 295 (2021) 113017, doi: 10.1016/j.jenvman.2021.113017.
[2] V.K. Gupta, S. Agarwal, R. Ahmad, A. Mirza, J. Mittal, Sequestration of toxic Congo red dye from aqueous solution using ecofriendly guar gum/activated carbon nanocomposite, Int. J. Biol. Macromol., 158 (2020) 1310–1318.
[3] M. Szlachta, P. Wojtowicz, Adsorption of methylene blue and Congo red from aqueous solution by activated carbon and carbon nanotubes, Water Sci. Technol., 6810 (2013) 2240–2248.
[4] R. Jain, P. Sharma, S. Sikarwar, J. Mittal, D. Pathak, Adsorption kinetics and thermodynamics of hazardous dye Tropaeoline 000 unto Aeroxide Alu C (nano alumina): a non-carbon adsorbent, Desal. Water Treat., 52 (2014) 7776–7783.
[5] V. Kumar, P. Saharan, A.K. Sharma, A. Umar, I. Kaushal, A. Mittal, Y. Al-Hadeethi, B. Rashad, Silver doped manganese oxide-carbon nanotube nanocomposite for enhanced dye-sequestration: isotherm studies and RSM modelling approach, Ceram. Int., 468 (2020) 10309–10319.
[6] S. Adhikari, S. Mandal, D. Sarkar, D.-H. Kim, G. Madras, Kinetics and mechanism of dye adsorption on WO_3 nanoparticles, Appl. Surf. Sci., 420 (2017) 472–482.
[7] C. Lei, M. Pi, B. Cheng, C. Jiang, J. Qin, Fabrication of hierarchical porous ZnO/NiO hollow microspheres for adsorptive removal of Congo red, Appl. Surf. Sci., 435 (2018) 1002–1010.
[8] P. Jha, R. Jobby, N.S. Desai, Remediation of textile azo dye acid red 114 by hairy roots of Ipomoea carnea Jacq. and assessment of degraded dye toxicity with human keratinocyte cell line, J. Hazard. Mater., 311 (2016) 158–167.
[9] A. Ahmad, S.H. Mohd-Setapar, C.S. Chuong, A. Khatoon, W.A. Wani, R. Kumar, M. Rafatullah, Recent advances in new generation dye removal technologies: novel search for approaches to reprocess wastewater, RSC Adv., 539 (2015) 30801–30818.
[10] C. Lei, M. Pi, P. Kuang, Y. Guo, F. Zhang, Organic dye removal from aqueous solutions by hierarchical calcined Ni-Fe layered double hydroxide: isotherm, kinetic and mechanism studies, J. Colloid Interface Sci., 496 (2017) 158–166.
[11] S. Patra, E. Roy, R. Madhuri, P.K. Sharma, Agar based bimetallic nanoparticles as high-performance renewable adsorbent for removal and degradation of cationic organic dyes, J. Ind. Eng. Chem., 33 (2016) 226–238.
[12] M.T. Yagub, T.K. Sen, S. Afroze, H.M. Ang, Dye and its removal from aqueous solution by adsorption: a review, Adv. Colloid Interface Sci., 209 (2014) 172–184.
[13] M.A.M. Salleh, D.K. Mahmoud, W.A.W.A. Karim, A. Idris, Cationic and anionic dye adsorption by agricultural solid wastes: a comprehensive review, Desalination, 280 (2011) 1–13.
[14] Z. Zou, Y. Tang, C. Jiang, J. Zhang, Efficient adsorption of Cr(VI) on sunflower seed hull derived porous carbon, J. Environ. Chem. Eng., 32 (2015) 898–905.
[15] X. Jin, B. Yu, Z. Chen, J.M. Arocena, R.W. Thring, Adsorption of Orange II dye in aqueous solution onto surfactant-coated zeolite: characterization, kinetic and thermodynamic studies, J. Colloid Interface Sci., 435 (2014) 15–20.
[16] G.Z. Kyzas, E.A. Deliyanni, D.N. Bikiaris, A.C. Mitropoulos, Graphene composites as dye adsorbents: review, Chem. Eng. Res. Des., 129 (2018) 75–88.
[17] A.E. Burakov, E.V. Galunin, I.V. Burakova, A.E. Kucherova, S. Agarwal, A.G. Tkachev,V.K. Gupta, Adsorption of heavy metals on conventional and nanostructured materials for wastewater treatment purposes: a review, Ecotoxicol. Environ. Saf., 148 (2018) 702–712.
[18] K.C. Lai, L.Y. Lee, B.Y.Z. Hiew, S. Thangalazhy-Gopakumar, S. Gan, Environmental application of three-dimensional graphene materials as adsorbents for dyes and heavy metals: review on ice-templating method and adsorption mechanisms, J. Environ. Sci., 79 (2019) 174–199.
[19] H. Seddighi, A.K. Darban, A. Khanchi, J. Fasihi, J. Koleini, LDH(Mg/Al:2)@montmorillonite nanocomposite as a novel anion-exchanger to adsorb uranyl ion from carbonate-containing solutions, J. Radioanal. Nucl. Chem., 314 (2017) 415–427.
[20] Y. Xu, G. Ke, J. Yin, W. Lei, P. Yang, Synthesis of thiol-functionalized hydrotalcite and its application for adsorption of uranium(VI), J. Radioanal. Nucl. Chem., 319 (2019) 791–803.
[21] W. Yao, S. Yu, J. Wang, Y. Zou, S. Lu, Y. Ai, N.S. Alharbi, A. Alsaedi, T. Hayat, X. Wang, Enhanced removal of methyl orange on calcined glycerol-modified nanocrystallined Mg/Al layered double hydroxides, Chem. Eng. J., 307 (2017) 476–486.
[22] S. Yu, X. Wang, Z. Chen, J. Wang, S. Wang, T. Hayat, X. Wang, Layered double hydroxide intercalated with aromatic acid anions for the efficient capture of aniline from aqueous solution, J. Hazard. Mater., 321 (2017) 111–120.
[23] Y. Zhou, Z. Liu, A. Bo, T. Tana, X. Liu, F. Zhao, S. Sarina, M. Jia, C. Yang, Y. Gu, H. Zheng, H. Zhu, Simultaneous removal of cationic and anionic heavy metal contaminants from electroplating effluent by hydrotalcite adsorbent with disulfide (S^{2-}) intercalation, J. Hazard. Mater., 382 (2020) 121111, doi: 10.1016/j.jhazmat.2019.121111.

[24] Y. Zou, X. Wang, Y. Ai, Y. Liu, J. Li, Y. Ji, X. Wang, Coagulation behavior of graphene oxide on nanocrystallined Mg/AI layered double hydroxides: batch experimental and theoretical calculation study, Environ. Sci. Technol., 507 (2016) 3658–3667.
[25] W. Linghu, H. Yang, Y. Sun, G. Sheng, Y. Huang, One-pot synthesis of LDH/GO composites as highly effective adsorbents for decontamination of U(VI), ACS Sustainable Chem. Eng., 56 (2017) 5608–5616.
[26] J. Wang, X. Wang, L. Tan, Y. Chen, T. Hayat, J. Hu, A. Alsaedi, B. Ahmad, W. Guo, X. Wang, Performances and mechanisms of Mg/Al and Ca/Al layered. double hydroxides for graphene oxide removal from aqueous solution, Chem. Eng. J., 297 (2016) 106–115.
[27] W. Yao, J. Wang, P. Wang, X. Wang, S. Yu, Y. Zou, J. Hou, T. Hayat, A. Alsaedi, X. Wang, Synergistic coagulation of GO and secondary adsorption of heavy metal ions on Ca/Al layered double hydroxides, Environ. Pollut., 229 (2017) 827–836.
[28] Y. Zou, X. Wang, Z. Chen, W. Yao, Y. Ai, Y. Liu, T. Hayat, A. Alsaedi, N.S. Alharbi, X. Wang, Superior coagulation of graphene oxides on nanoscale layered double hydroxides and layered double oxides, Environ. Pollut., 219 (2016) 107–117.
[29] W.S. Putro, T. Kojima, T. Hara, N. Ichikuni, S. Shimazu, Acceptorless dehydrogenation of alcohols using Cu-Fe catalysts prepared from Cu-Fe layered double hydroxides as precursors, Catal. Sci. Technol., 812 (2018) 3010–3014.
[30] X. Wang, Y. Tuo, Y. Zhou, D. Wang, S. Wang, J. Zhang, Ta-doping triggered electronic structural engineering and strain effect in NiFe LDH for enhanced water oxidation, Chem. Eng. J., 403 (2021) 126297, doi: 10.1016/j.cej.2020.126297.
[31] S. Mondal, P. Chakraborty, P. Bairi, D.P. Chatterjee, A.K. Nandi, Light induced E-Z isomerization in a multi-responsive organogel: elucidation from H^{-1} NMR spectroscopy, Chem. Commun., 51 (2015) 10680–10683.
[32] J.A. Prithi, N. Rajalakshmi, G.R. Rao, Nitrogen doped mesoporous carbon supported Pt electrocatalyst for oxygen reduction reaction in proton exchange membrane fuel cells, Int. J. Hydrogen Energy, 439 (2018) 4716–4725.
[33] F. Ning, M. Shao, S. Xu, Y. Fu, R. Zhang, M. Wei, D.G. Evans, X. Duan, TiO_2/graphene/NiFe-layered double hydroxide nanorod array photoanodes for efficient photoelectrochemical water splitting, Energy Environ. Sci., 98 (2016) 2633–2643.
[34] S. Wang, J. Zhu, S. Zhang, X. Zhang, F. Ge, Y. Xu, The catalytic degradation of nitrobenzene by the Cu-Co-Fe-LDH through activated oxygen under ambient conditions, Dalton Trans., 49 (2020) 3999–4011.
[35] X. Rong, F. Qiu, J. Qin, H. Zhao, J. Yan, D. Yang, A facile hydrothermal synthesis, adsorption kinetics and isotherms to Congo red azo-dye from aqueous solution of NiO/graphene nanosheets adsorbent, J. Ind. Eng. Chem., 26 (2015) 354–363.
[36] Y. Zheng, B. Cheng, W. You, J. Yu, W. Ho, 3D hierarchical graphene oxide-NiFe LDH composite with enhanced adsorption affinity to Congo red, methyl orange and Cr(VI) ions, J. Hazard. Mater., 369 (2019) 214–225.
[37] D. Maiti, S. Mukhopadhyay, P.S. Devi, Evaluation of mechanism on selective, rapid, and superior adsorption of Congo red by reusable mesoporous α-Fe_2O_3 nanorods, ACS Sustainable Chem. Eng., 512 (2017) 11255–11267.